frontiers | Frontiers in Earth Science

TYPE Original Research
PUBLISHED 08 September 2023
DOI 10.3389/feart.2023.1258022

OPEN ACCESS

EDITED BY
Zhanwu Lu,
Chinese Academy of Geological Sciences, China

REVIEWED BY
Yun Chen,
Chinese Academy of Sciences (CAS), China
Qiang Xu,
Chinese Academy of Sciences (CAS), China
Zhen Liu,
Chengdu University of Technology, China

*CORRESPONDENCE
Xiao Xu,
xuxiao8@mail.sysu.edu.cn
Jiahao Yu,
Yuyujh23@mail2.sysu.edu.cn

RECEIVED 13 July 2023
ACCEPTED 29 August 2023
PUBLISHED 08 September 2023

CITATION
Xiang B, Xu X, Yu J, Guo X, Wu Y, Li C, Wu J, Tong X and Luo X (2023), Late Miocene landform construction in east-southern Tibet: seismic evidence and a synthetic review.
Front. Earth Sci. 11:1258022.
doi: 10.3389/feart.2023.1258022

Late Miocene landform construction in east-southern Tibet: seismic evidence and a synthetic review

Bo Xiang[1,2], Xiao Xu[1,2]*, Jiahao Yu[1,2]*, Xiaoyu Guo[1,2], You Wu[1,2], Chunsen Li[1,2], Jiajie Wu[1,2], Xiaofei Tong[1,2] and Xucong Luo[1,2]

[1]School of Earth Sciences and Engineering, Sun Yat-sen University, Zhuhai, China, [2]Southern Marine Science and Engineering Guangdong Laboratory (Zhuhai), Zhuhai, China

The north-south striking landform perpendicular to the dominant collision zone between the Indian and Eurasian plates was constructed in east-southern Tibet (EST) during the Late Miocene. The building processes remain ambiguous, partly owing to the lack of recognition of crustal-scale architecture. Here we deployed an east-west-oriented 120 km-long short-period dense array across the northwestern corner of EST. Results from P-wave receiver functions show a mid-crustal ductile detachment atop the crystalline basement of the eastern Lhasa terrane that has displaced the overlying crust including the upper part of the Yardong-Gulu Rift (YGR) eastward for about 100 km and an offset Moho geometry left behind beneath the Nyainqentanghla Range. Combined previous studies on the vertical heterogeneity in crustal strength beneath the YGR, a synthetic view implies a decoupled crustal architecture of EST to respond the dynamic interactions between the eastward extrusion of the Tibetan Plateau and the northward penetration of the Indian plate that constitutes the Eastern Himalayan Syntaxis. The integrated processes eventually brought active landform construction in the plateau's interior and partly contributing to the contemporaneous intensification of monsoon in SE Asia.

KEYWORDS

receiver function, Yardong-Gulu rift, dense seismic array, decoupled crust, east-southern Tibet

1 Introduction

Globally, an orogenic process generally leads to linear mountain construction that is parallel to the dominant collision zone. However, in the Tibetan Plateau, besides its prominently high topography and low relief, a very unique morphology is presented in the east-southern Tibetan Plateau, where the high Nyainqentanghla Range (NR) (peak at 7,016 m) and the Yardong-Gulu rift zone (YGR) strike in a northeasterly direction that is nearly perpendicular to the dominant collision zone between the Indian and Eurasian plates (Figure 1A). More interestingly, the onset of the mountain construction along the Nyainqentanghla Range and rifting along the YGR has been geochronologically constrained to take place during the Late Miocene (Pan and Kidd, 1992; Harrison et al., 1995; Kapp, 2005; Chevalier et al., 2020), a time that post-dated the time when southern Tibet has been unchanged in altitude since the Mid-Miocene (Spicer et al., 2003). Moreover, uplift of the Tibetan Plateau, driven by the collision of India, is widely regarded to rise as a

coherent entity (Tapponnier et al., 2001). Thus, what drove the northeast-oriented topographic construction has been ambiguous, as to how the deep process of Indian penetration is coupled to the deformation in the shallower crust in east-southern Tibet remains unclear.

While plate tectonic theory provides a general explanation of geophysical and surface structural features, the details of how deep geodynamics and other kinematic parameters of continent-continent collision cause specific features at local scales are uncertain. Many studies have interpreted surface structures within the Tibetan plateau as accommodating lateral extrusion or anisotropic features as highlighting mantle geodynamics (England and Houseman, 1989; Royden et al., 1997; Clark and Royden, 2000; Beaumont et al., 2001; Shapiro et al., 2004). Few studies have addressed the mechanical origin of surface structures within a consistent framework of kinematic evolution, and crustal-scale responses are missing in the prevailing explanations. The east-southern Tibetan Plateau is an excellent setting for connecting surface features with regional mechanisms due to the post collisional landform construction and, meanwhile, the long term and salient effects of the advancing and deeply rooted front of the Indian slab around the Eastern Himalayan Syntaxis.

In this study, we describe a 120 km-long short-period dense array profile collected across the northwestern corner of east-southern Tibet. The combined image is interpreted along with previous geologic and geophysical data to evaluate regional kinematic processes associated with the ongoing eastward extrusion of the Tibetan Plateau and indentation of the Indian Plate around the Eastern Himalayan Syntaxis. This Late Miocene chaotic but active tectonic events in EST will thus shed new lights on

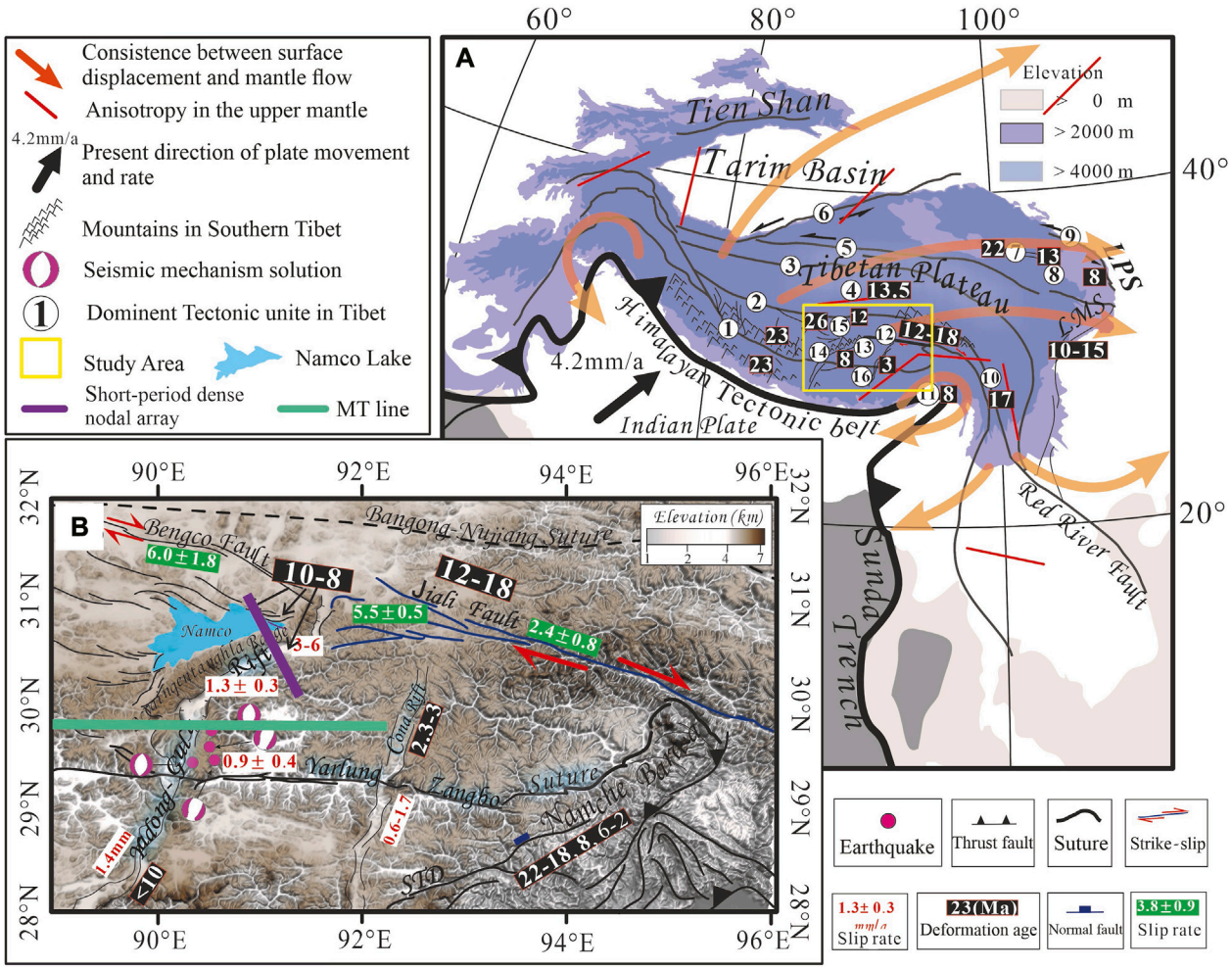

FIGURE 1
Schematic clockwise rotation of the Tibetan Plateau and overview of the study area; **(A)** shows the direction of clockwise rotation of different parts of the Tibetan Plateau (shown by yellow arrows); black arrows indicate GPS velocities relative to the stable Asian and European continents (Liang et al., 2013); the yellow box shows the study area shown in the upper right figure; ①Yarlung-Zangbo suture,②:Banggong-Nujiang suture,③:Jinsha suture,④:Qiangtang block,⑤:Kunlun fault,⑥:Altyn Tagh fault,⑦:Jishi Mountain,⑧:Laji Mountain,⑨:Haiyuan fault,⑩:Xianshuihe fault,⑪:Eastern Himalayan Syntaxis,⑫:Jiali fault,⑬:Yardong-Gulu rift, ⑭:Nyainqentanghla range,⑮:Namco lake,⑯:Cuona rift; **(B)** shows the geological formations, initial tensioning time (Ma) and main tectonic activity rate (mm/a) of the study area; the initial The initial rift age (Ma) of each rift is marked in purple (Harrison et al., 1995; Maheo et al., 2007); the black markers are the activity rates of the strike-slip fractures (mm/a), among which the inferred activity rates are for the Jiali rift zone (mm/a) and the rest are the present-day activity rates (mm/a) (Armijo et al., 1989; Hager, 2014; Ha et al., 2019); the white markers are the displacements of the Jiali rift to the Yardong-Gulu rift.

understanding tectonic interactions between India and Eurasia after amalgamation.

2 Geological background

The currently ongoing India-Eurasia collision uplifted the Himalayan-Tibetan orogenic belt and further constructed the whole Tibetan Plateau to its current elevation (Blisniuk et al., 2001). The Lhasa terrane is located along the collision front between the Indian and Eurasian Plates (Figure 1A) and all collision-related events will thus be recorded within it. Previous geochemical and petrological studies have divided the Lhasa terrane into three east-west oriented sub-terranes, including the central Lhasa micro-continent, and the southern and northern juvenile sub-terranes that have gone through episodic magmatism (Zhu et al., 2011). These three subterranes are separated from south to the north, respectively, by the east-west-striking Luobadui-Milashan fault and the Shiquanhe-Namco fault (Zhu et al., 2011). Meanwhile, north-striking rift systems are widespread within the Lhasa terrane, which were initiated owing to slab tear of the subducting Indian plate (Hou et al., 2006; Chen et al., 2015; Guo et al., 2018) and subsequent eastward extrusion of the plateau during the Middle Miocene (Blisniuk et al., 2001; Lease et al., 2011). Controlled by the arc structure that protrudes to the south of the Yarlung-Zangbo suture (YZS), orientation of the rift system in the Lhasa terrane changes from a northwesterly direction in the west to a northeasterly direction in the east (Figure 1A).

In the eastern Lhasa terrane (east-southern Tibet, EST), it shows a typically different topography relative to other parts of the Lhasa terrane (Figure 1B). First of all, there is the largest rift zone, i.e., the NE-striking Yardong-Gulu rift system (YGR). Along its footwall, it exhumed the highest NE-striking Nyainqentanghla Range (NR) at 10–8 Ma in the plateau's interior (Pan and Kidd, 1992; Harrison et al., 1995; Kapp, 2005; Chevalier et al., 2020). The NR is in turn bounded to the west by the Namco Lake (Figure 1B), the second largest lake in the plateau's interior that was originated at 8 Ma as being a pull-apart basin (Schulze, 2021). Morphologically, both the NR and YGR change coherently from a northerly direction to northeasterly and easterly direction from south to the north (Figure 1B). Additionally, the YGR progressively decreases in vertical slip rate southward from 3 to 6 mm/yr along the northern part to 1.3 ± 0.3 mm/yr in the south (Chevalier et al., 2020; Zuo et al., 2021). Coherently, the NR decreases in elevation along strike to the southwest where the trend changes to a northerly direction (Figure 1B). Field geology shows a SE-dipping low-angle normal fault with mylonites along the range front of the NR, while $^{40}Ar/^{39}Ar$ thermochronolgic studies have indicated the *in-situ* lower crust partial melting and an emplacement to the midcrust (Kapp, 2005). No features in association with core-complex are yet seen within the NR (Kapp, 2005), and the relationships resulting from the coherence in deformation between YGR and NR needs to be confirmed.

Besides the NR and YGR, there is the NE-striking Namche-Barwa Mountain Range (NBR) locating along the easternmost segment of the YZS to the south (Figure 1A). It is part of the subducted Indian crust and has contributed dominantly to construction of the Eastern Himalayan Syntaxis (EHS) (Xu et al., 2012). The NBR has experienced crustal-scale exhumation through the deep crust at 22–18 Ma to the shallower crust at 6–2 Ma (Xu et al., 2012). Rapid exhumation of the NBR was constrained to commence since ~8 Ma of Late Miocene in age (Ding et al., 2001). Moreover, the maximum compression stress in association with construction of the EHS from indentation of the Indian slab fans radially throughout the EST (Huchon et al., 1994; Schellart et al., 2019) (Figure 1A). To both northern and southern sides of the EST, there locates, respectively, the east-west striking YZS and the Jiali fault zone (Figure 1B). The dextral Jiali shear zone to the northern edge of EST possesses a faster slip rate of 5.0 ± 0.5 mm/yr in its westernmost segment, where cuts through the YGR, and then decreases to 2.4 ± 0.8 mm/yr in the middle part (Zhang et al., 2021). Thus, the northwestern corner of EST possesses more active tectonics relative to the other parts.

3 Data and methods

The P wave receiver function method is widely used to study the structure of the crust and upper mantle by inversion of broadband seismic station data (Langston, 1979; Kumar et al., 2006). The dense nodal array was employed in this study. The teleseismic waveforms used in this study were collected in the north section of the YGR from October to November 2019 (Figure 2A). The observation system was a nearly NW nodal array composed of 92 three-component nodes (Magseis Fairfield ZLand 3C) with 5 Hz corner frequency spaced at 1 km. Nodal seismometers record signals at higher frequencies than that of the broadband seismometers, which resulted in a higher theoretical vertical resolution (Wu et al., 2017). Moreover, the shorter station spacing improves the lateral resolution, compensating for fewer recorded teleseismic events (Tian et al., 2015). Numerous experiments have demonstrated that the receiver functions calculated from seismic data with dense nodal arrays can image more details than those by the broadband station (Leahy et al., 2012; Liu et al., 2017; Saikia et al., 2017; Ward and Lin, 2017; Farrell et al., 2018; Liu et al., 2018; Ringler et al., 2018; Sweet et al., 2018; Tian et al., 2021).

A total of 98 teleseismic events with Ms≥5.1 was recorded during the observation period of ~40 days. Poor quality dataset was removed by signal-to-noise ratio calculation and manual selection, and 32 available seismic events were retained (Figure 2B) (Ammon, 1991). The 60 s continuous waveforms, the 10 s before and 50 s after the theoretical P arrival time, had been resampled (100 Hz sample rate) to write the information of station and event. The frequencies of band pass filter were used between 0.1 and 8 Hz. The horizontal component (northern and eastern) had been rotated around the theoretical back azimuth angle into the radial and transverse system (Langston, 1979; Zhu, 2000a). A frequency domain deconvolution algorithm was used to calculate receiver functions from radial and vertical components of waveforms. Finally, the 2,709 high-quality RFs were calculated.

In order to highlight the regional crustal structure (Ward et al., 2018) and compare with the results from previous study (Zhang et al., 2013), the receiver functions were smoothed for a stacking radius window of 1 and 3 km (Figures 3B,C). The stacking of the RFs has a good consistence of the main structures with those obtained by broadband data, but also has more details. The common conversion

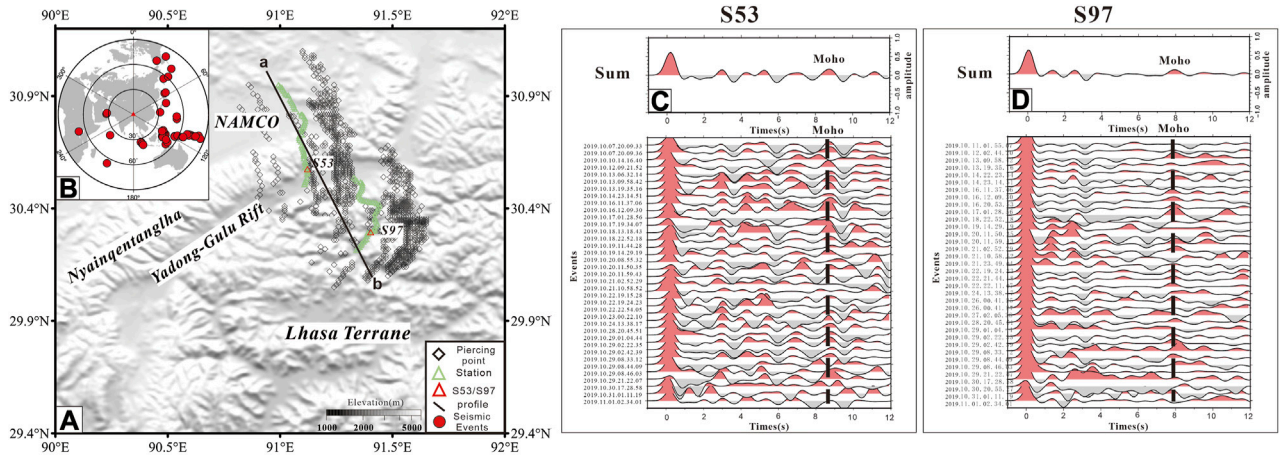

FIGURE 2
(A) the green triangles is the station deployment point; the black diamonds is the 70 km piercing point of RFs; the red triangles are the station locations in **(C, D)**, respectively; **(B)** the teleseismic distribution map used to calculate the receiver function; **(C, D)** The upper panel shows the superimposed RFs of different events at some stations of along the line, and the lower panel shows the arrangement of RFs of different events; the black dashed line marks the Pms transition phase that represents the occurrence of Moho.

point (CCP) stacking (Zhu, 2000a; Chen et al., 2005) was used to image the lithospheric structures (Figure 3D).

4 Results

The migrated receiver function image is shown in Figure 4A. Combined with previous studies on Moho depth from broadband receiver function (Zhang et al., 2013; Tian et al., 2015), the interface with high amplitude at 70–78 km in our study represents the Moho geometry. It is at depths of 78 km beneath the NR and then lifts to approx. 70 km to the east of the YGR (Figure 4B). More importantly, the Moho geometry is offset right beneath the NR (Figure 4B), a scenario that is consistent with Ps analysis for an identification of a weakening to disappearing Moho amplitude (Zhang et al., 2013). A sequence of weak interfaces with low amplitude are presented as well beneath the NR, which can be traced from the mantle depths, through the offset Moho, to the upper crust. They show strong amplitude against the overlying shallower crust. Additionally, a prominent intracrustal interface appears at depths of 50 km throughout the entire profile, which shows as being a low velocity layer in previous tomographic studies (Tian et al., 2015). This intracrustal interface appears with a typically weak amplitude of concave downward in the middle of the profile. Along with surface observations of the YGR, the RF imagery connecting the YGR with a sequence of interface terminations can be traced downward to merge with the identified intracrustal shear zone at approx. 50 km. On the other side, a sequence of strong interface terminations right beneath the NR is seen from depths of 50 km, through the offset Moho, downward to the mantle depth. At further deeper depths of approx. 120 km, combined with previous studies by Shi et al. (2015), the discrete strong negative interfaces on both sides of the YGR possibly represents the torn lithosphere-asthenosphere boundary (Figure 4B), but the western segment beneath the NR is much deeper than that of the eastern segment.

Previous tomographic studies by Liang et al. (2016) has documented the significant lithospheric-scale thermal influence from the asthenospheric upwelling beneath this NR (Figure 5A). We superimpose the tomographic results onto our RF results (Figure 5B) and a synthetic view drives to interpret that the domain outlined by weak interfaces may have been affected by the tectonothermal activities from the upwelling asthenosphere through the torn LAB dominantly beneath the NR (Figure 5C). Meanwhile, the original ductile normal fault of the YGR is seen to have cut through into the mantle depth, which was later displaced into two parts by the intracrustal detachment atop the crystalline basement (Figure 5D). The overlying segment has moved eastward for about 100 km from the original segment (Figure 5D). Meanwhile, the concave downward interface beneath the NR is highly derived from stress accumulation to accommodate the uplift of the NR.

5 Discussion on kinematic mechanism driving active landform construction

Previous tomographic studies have outlined a weakly decoupled lithospheric extension of southern Tibet (Tian et al., 2015). In our study, the overall RF imagery further displays a 100 km-eastward displacement of the upper part of the YGR original normal fault and the dominant influence to the mid-to-lower crust beneath the NR and adjacent regions on both sides (Figures 5D, 6A). This displacement between the surface exposure and the Moho offset is however not evidenced beneath the southern part of the YGR in the MT profile (Wang et al., 2017) (Figures 1B, 6B). The overall architecture implies a geodynamic adjustment from extension through compressive stress to extension for landform construction during extrusion. The next step is to formulate the mechanism behind.

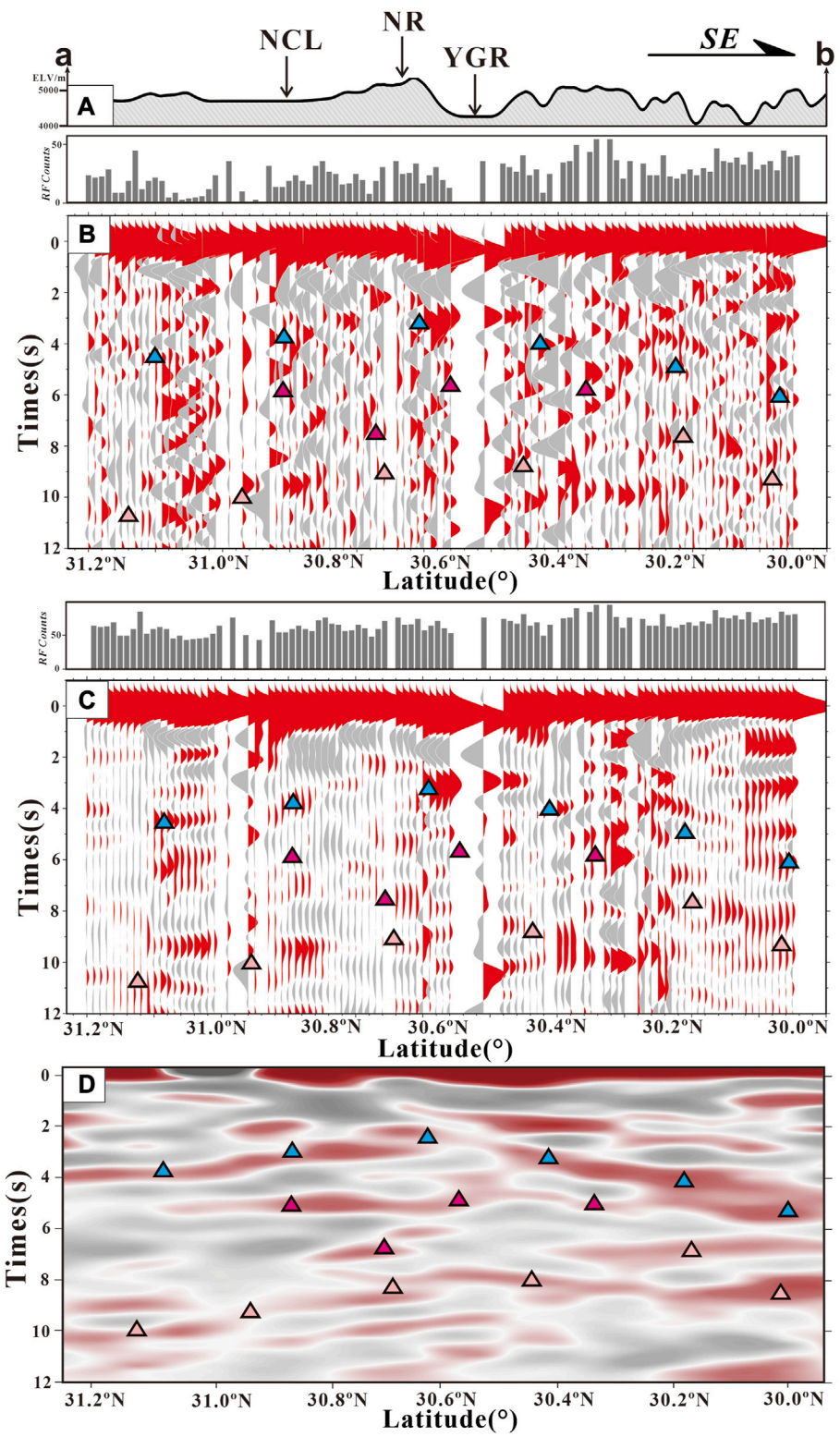

FIGURE 3
(A) Topographic elevation map between survey line, NR: Nyainqentanglha Range. YGR: Yardong-Gulu rift. NCL: Namco Lake; **(B)** and **(C)** are the results of RFs superimposed with a Gaussian filter parameter value of 2.5 for a superimposed distance window of 0 km and 3 km radius for all events; **(D)** is the depth images of all event RFs were superimposed using CCP. To compare the results of different methods, blue, purple and red triangles are used to represent the crustal features (upper crust, middle crust and Moho).

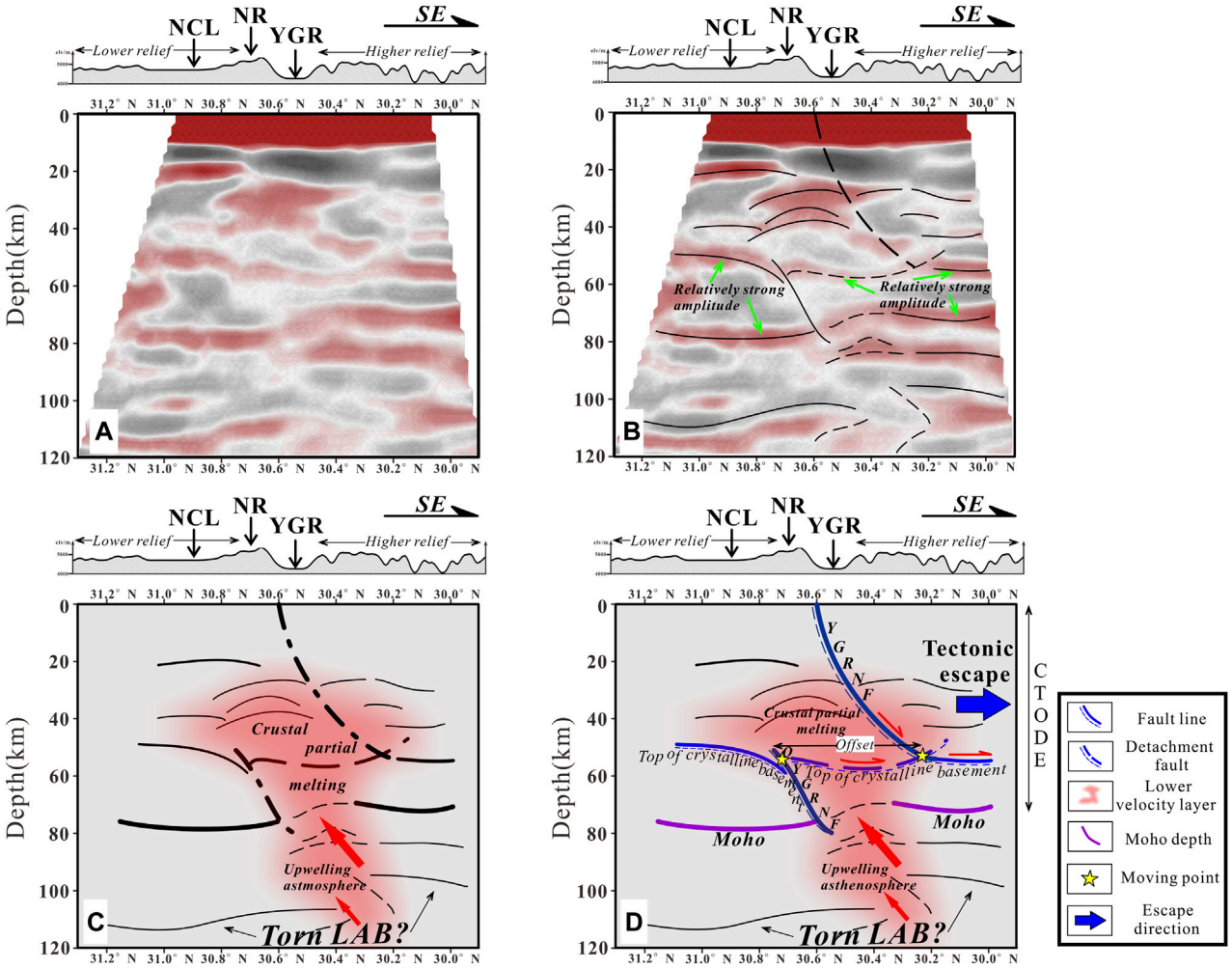

FIGURE 4
(A) is the migration image of the receiver function of the survey line; **(B)** marked with the main seismic phase on the image.

5.1 Regional geodynamics

Previous seismic studies have clearly outlined the variation in underthrusting geometry of the Indian plate (Li et al., 2008; Zhao et al., 2010; Replumaz et al., 2013; Guo et al., 2018). The underthrusting Indian slab exhibits nearly horizontal geometry beneath the western Tibetan Plateau, where has extended northward to touch the southern edge of the Tarim Basin. Thereafter, the underthrusting Indian slab longitudinally increases in underthrusting angle and decreases in horizontal advance distance toward the east. To the easternmost segment beneath the Eastern Himalayan Syntaxis (EHS), the underthrusting Indian slab terminates to the southern Yarlung-Zangbo suture zone and no further northward advance is seen (Li et al., 2008). Tomographic studies identify the limited northward extent of the Indian penetration beneath the EHS and Asian origin of the lithosphere beneath southeastern Tibet (Li et al., 2008). As the subduction resistance increased from the Eurasian lithosphere, retrograde metamorphism of the HP/UHP metamorphosed Indian crust occurred at eastern corner of the Himalayas (Xu et al., 2012). The top-to-the south unroofing progressively affected the eastward extrusion of the southeastern Tibetan crust, which started from the deeper depth at 22–18 Ma (Xu et al., 2012) and then the shallow crust until 6 Ma (Xu et al., 2012). It worked as a backstop to resist temporally the further eastward extrusion of east-southern Tibet. The Indian plate is undergoing collision with Eurasia in a counterclockwise pattern (Todrani et al., 2022). To the east of India-Eurasia collision zone, combined with the slab retreat of the Indo-Australian plate along the Sunda Trench to the east (Pubellier and Morley, 2014), counterclockwise advance of the Indian plate resulted in active construction of the EHS and radial orientation of the maximum horizontal component of the compressive stress in a fan geometry around the EHS (Gan et al., 2007; Schellart et al., 2019; Todrani et al., 2022) (Figure 1A).

With the onset of the plateau-wide collapse since the Middle Miocene (Blisniuk et al., 2001; Lease et al., 2011), the wide-spaced rift grabens in southern Tibet was triggered along the weak zones from north to the south, beneath which the

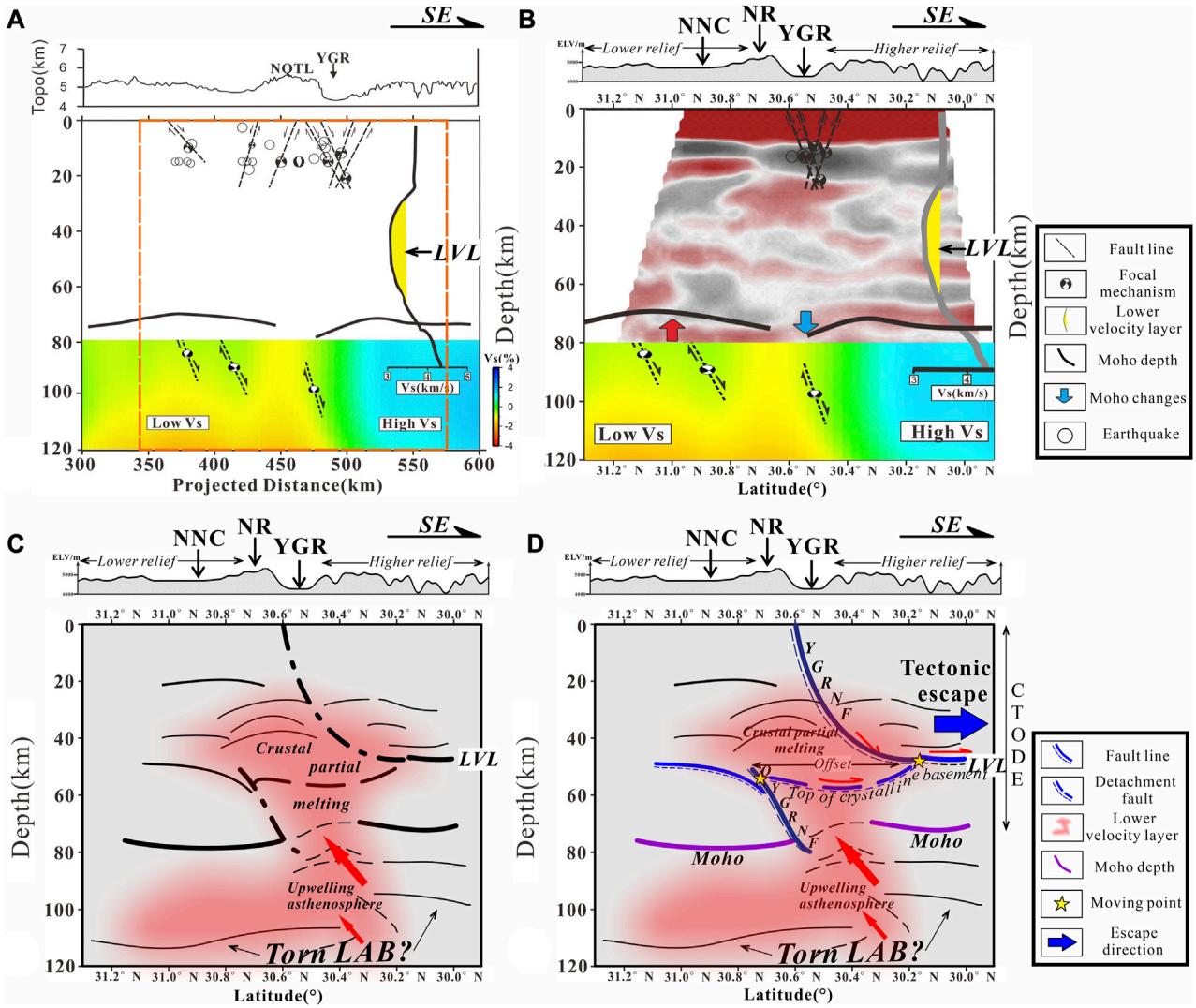

FIGURE 5
(A) Tomographic studies by Liang et al. (2016), the thick black solid line is the calculated Moho depth, the color chart below shows the S-wave velocity; **(B)** Consistence between previous tomographic results with our RF results for outlining crustal-scale features; **(C)** Crustal partial melting after upwelling asthenosphere; **(D)** Delineation of an intra-crustal shear zone for a decoupled crustal architecture beneath east-southern Tibet. NR, Nyainqentanglha Range. YGR, Yardong-Gulu rift. NCL, Namco Lake. LVL, Low velocity layer.

subducting Indian slab was torn as a result of variation in dipping angle (Chen et al., 2015; Guo et al., 2018). The process was accommodated with a crustal-scale deformation of the rifting events (Hou et al., 2006; Chen et al., 2015; Guo et al., 2018), which is additionally supported by exposure of the ultrapotassic/potassic rocks from the mantle depth along the rift zones (Liu et al., 2014; Guo et al., 2015). In a larger context, the eastward extrusion of EST confronts a progressive development of the maximum compressive stress that fans systematically around the EHS. This process resulted in an overall 56%–78% less extrusion rate of the southern YGR than that of the northern YGR (Chevalier et al., 2020), indicating a decreasing compressive stress field and therefore an increasing extrusion from south close to the EHS further away to the north. Thereafter, diversity in topographic construction will be created in EST.

5.2 Landform construction of the east-southern Tibetan Plateau

Figure 7 presents a sketch showing kinematic processes in landform construction of northern EST from an integrated analysis of both the crustal architecture from our newly obtained seismic profile and previous studies in geophysics and petrology.

Previous tomographic studies have identified the weakly coupled extension of southern Tibet (Tian et al., 2015) when southern Tibet possessed an unchanged altitude at 15 Ma (Spicer et al., 2003) (Figure 7A). The plateau-wide eastward extrusion took place at 13.5 Ma (Blisniuk et al., 2001; Lease et al., 2011), which drove crustal-scale extension along the YGR where there was a weak zone left over by slab tear of the subducting Indian plate (Hou et al., 2006; Chen et al., 2015). Contemporaneously to the eastern corner of the collision zone, the EHS was actively constructed (Xu et al., 2012)

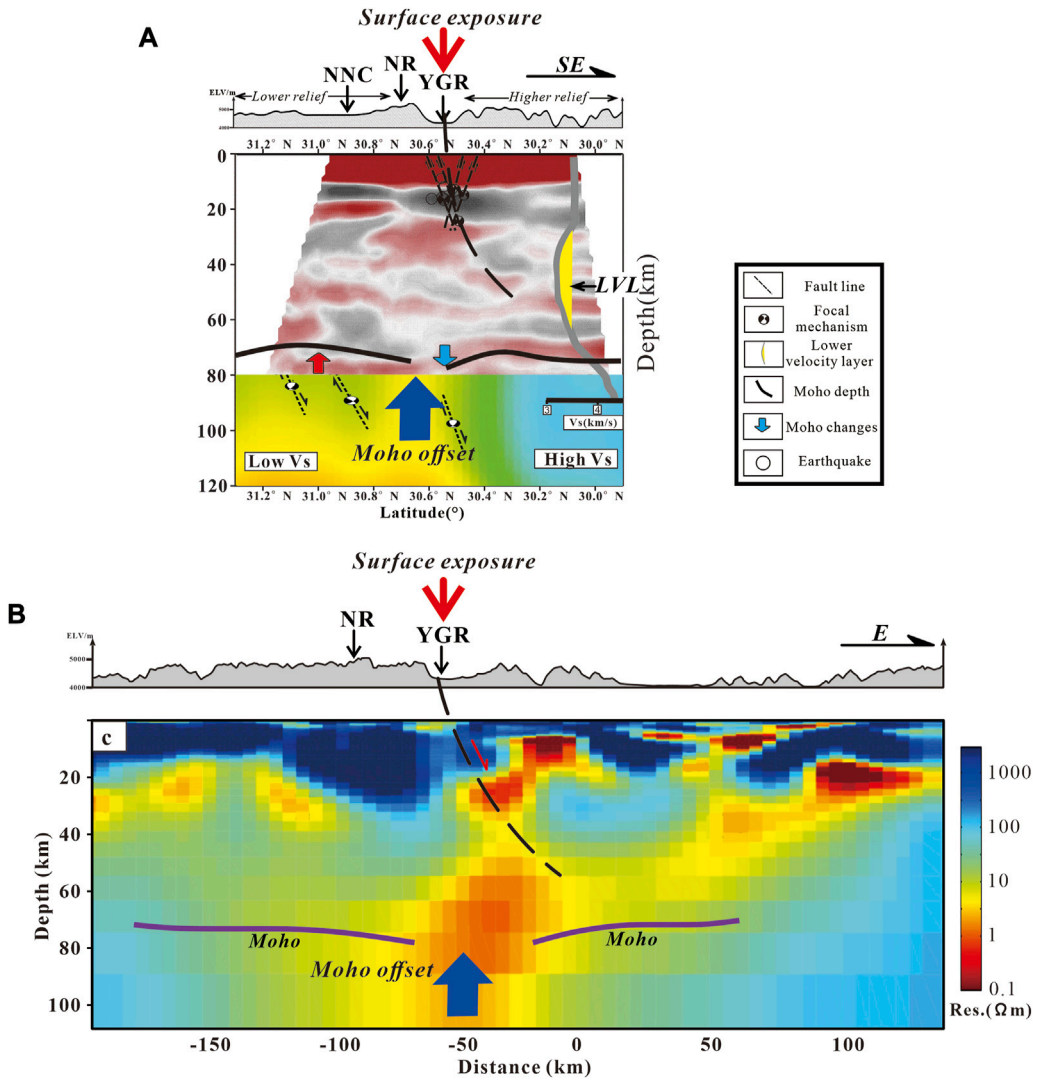

FIGURE 6
Comparison on the displacement between the surface exposure of the Yardong-Gulu rift and the Moho offset. **(A)** Results from a combined tomographic survey line (Tian et al., 2015) and this study across the northern segment of the Yardong-Gulu rift, **(B)** results from the MT survey line across the southern segment of the Yardong-Gulu rift (Wang et al., 2017).

in accommodating counterclockwise collision of the Indian plate with the Eurasian plate (Todrani et al., 2022). The compressive stress that fans radially (Huchon et al., 1994) progressively developed upward from the deeper depths (Xu et al., 2012), which worked as a backstop that brought stress accumulation in the lower crust (Figure 7B). Continuous eastward extrusion in the upper crust above the intracrustal shear zone led to decoupled displacement between the lower and upper crust along the intracrustal shear zone owing to the vertical heterogeneity in crustal strength beneath the NR (Zhang et al., 2013) (Figure 7B). Consequently, the displacement seen in our RF imagery might have taken place dominantly during the time interval when the growing EHS reached the lower crust of EST (Figure 7C). Coming along with the complete construction of the EHS, a backstop was fully developed to temporally block the whole extrusion of the EST, a process that resulted in stress accumulation to lift the NR owing to its thermally weakened crust by upwelled asthenosphere (Figure 7D). The intracrustal shear zone appears concave-downward in geometry in the resultant RF imagery as being an indicator for stress accumulation beneath the NR. In this hypothesis, we assume stress accumulation occurred syn- or post-dating intracrustal detached displacement, because there was no condition for a crustal-scale stress accumulation prior to complete exposure of the EHS. Shortly after, the EST found a new way to undergo clockwise rotation around the EHS. The whole process drove more extension along the northern YGR relative to that of the southern part (Figure 7E), and both the NR and YGR change northward from a northerly direction to northeasterly and easterly direction. Overall, tectonic interactions between plateau-wide eastward extrusion and progressive construction of the EHS have eventually created the unique landform in SE Tibet, including the typically high NR in the plateau's interior. Moreover, the

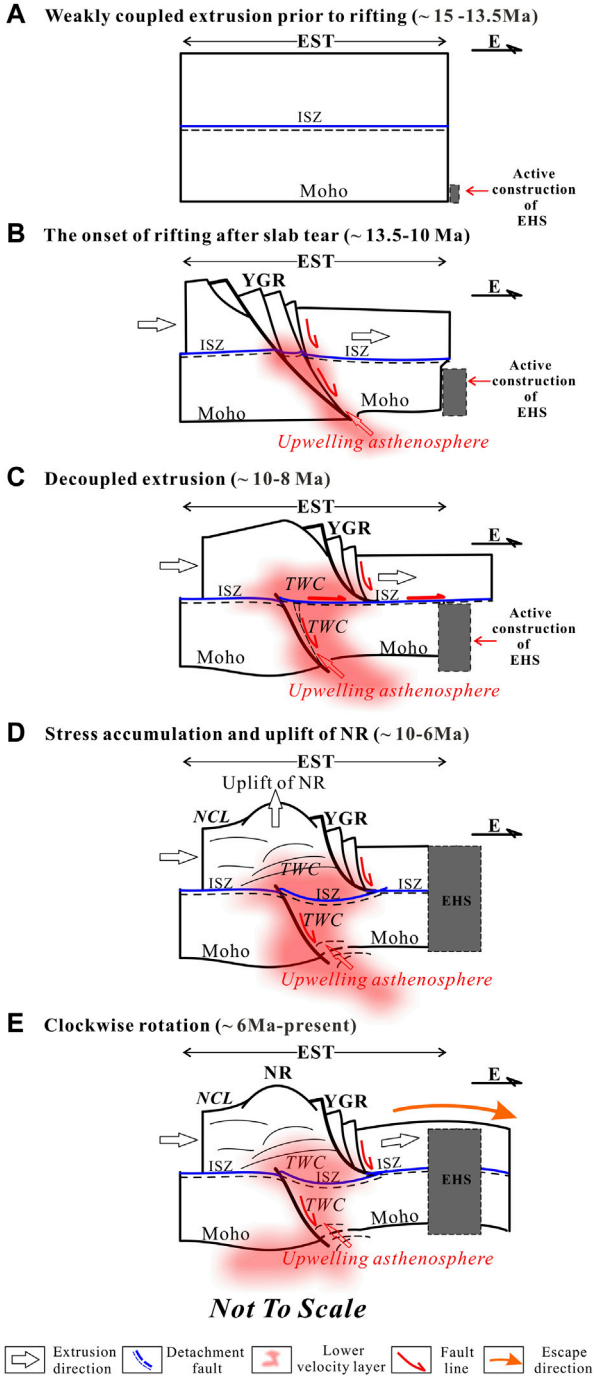

FIGURE 7
Kinematic interactions between eastward extrusion in east-southern Tibet and active construction of the Eastern Himalayan Syntaxis for mechanism driving diversity in surface topography in east-southern Tibet since Late Miocene (see context for more details). EST, East-southern Tibet; EHS, Eastern Himalayan Syntaxis; ISZ, Intracrustal shear zone; YGR, Yardong-Gulu Rift; TWC, Thermally weakened crust; NCL, Namco Lake.

mountain building within east-southern Tibet at 8 Ma could have partly contributed to the contemporaneously enhanced monsoon in the SE Asia (An et al., 2001).

6 Conclusion

Southern Tibet has remained in a constant elevation since 15 Myr ago (Spicer et al., 2003), while rapid uplift of the Nyainqentanglha Mountain Range (NR) in east-southern Tibet (EST) occurred around 10–8 Ma (Harrison et al., 1995; Ding et al., 2001; Kapp, 2005; Xu et al., 2012). Meanwhile, monsoon in SE was enhanced about 10–8 Myr ago, owing to the contemporaneous increase in elevation of the Tibetan Plateau (An et al., 2001). The driving mechanism for this puzzling topographic uplift in the plateau's interior and tectonic interactions with climate change remains unclear. In this study, first step toward solving this problem is to have obtained a 120 km-long crustal-scale seismic profile across the northern Yardong-Gulu rift zone (YGR). The results show the obvious offset Moho beneath the NR is 100 km west away from the surface exposure of the YGR. A mid-crustal detached shear zone appears to displace the original normal shear zone of the YGR into two parts and the upper part was displaced eastward. Moreover, seismic features indicate uplift of the NR was associated with stress accumulation above the detachment shear zone syn-or post-dating the decoupled extrusion. Considering the eastward extrusion of the plateau and progressive northward compression from penetration of the Indian slab, we believe their tectonic interactions are the key responsible for this diversity in surface structures. As a result, approx. 56%–78% less extrusion rate of southern segment of YGR was produced than that of the northern segment (Chevalier et al., 2020) and more stress accumulated in the northeastern part of EST to increase the elevation. That resulted in the maintenance of the regional southwest-flowing of the Lhasa river in the northeastern EST, although there is active surface construction to the south along the Yarlung-Zangbo suture zone by the intense collision between India and Eurasia (Laskowski et al., 2019) and could have also partly contributed to the enhanced monsoon in the SE Asia (An et al., 2001).

Data availability statement

The datasets presented in this study can be found in online repositories. The names of the repository/repositories and accession number(s) can be found below: https://doi.org/10.5281/zenodo.6480794.

Author contributions

BX: Conceptualization, Data curation, Methodology, Writing–original draft. XX: Conceptualization, Data curation, Methodology, Writing–review and editing. JY: Data curation, Investigation, Methodology, Writing–review and editing. XG: Conceptualization, Data curation, Funding acquisition, Investigation, Resources, Supervision, Writing–review and editing. YW: Data curation, Methodology, Writing–review and editing. CL: Data curation, Methodology, Writing–review and editing. JW: Data curation, Methodology, Writing–review and editing. XT: Data curation, Methodology, Writing–review and editing. XL: Data curation, Methodology, Writing–review and editing.

Funding

This study was financially supported by the National Natural Science Foundation of China (Grant No 42325402, 41874102, 42274120, 41974097) and the Second Tibetan Plateau Scientific Expedition and Research Program (STEP) (2019QZKK0701).

Acknowledgments

We want to thank all reviewers and authors for their contributions to this Research Topic. We also thank the entire Frontiers in Earth Science team for their dedicated effort in guiding the revision and detailed editing of the papers on the Research Topic.

Conflict of interest

The authors declare that the research was conducted in the absence of any commercial or financial relationships that could be construed as a potential conflict of interest.

Publisher's note

References

Ammon, C. J. (1991). The isolation of receiver effects from teleseismic P waveforms. *Bull. Seismol. Soc. Am.* 81 (6), 2504–2510. doi:10.1785/bssa0810062504

An, Z., Kutzbach, J. E., Prell, W. L., and Porter, S. C. (2001). Evolution of Asian monsoons and phased uplift of the Himalaya–Tibetan plateau since Late Miocene times. *Nature* 411 (6833), 62–66. doi:10.1038/35075035

Armijo, R., Tapponnier, P., and Han, T. (1989). Late Cenozoic right-lateral strike-slip faulting in southern Tibet. *J. Geophys. Res. Solid Earth* 94 (B3), 2787–2838. doi:10.1029/jb094ib03p02787

Beaumont, C., Jamieson, R. A., Nguyen, M. H., and Lee, B. (2001). Himalayan tectonics explained by extrusion of a low-viscosity crustal channel coupled to focused surface denudation. *Nature* 414 (6865), 738–742. doi:10.1038/414738a

Blisniuk, P. M., Hacker, B. R., Glodny, J., Ratschbacher, L., Bi, S., Wu, Z., et al. (2001). Normal faulting in central Tibet since at least 13.5 Myr ago. *Nature* 412 (6847), 628–632. doi:10.1038/35088045

Chen, L., Wen, L., and Zheng, T. (2005). A wave equation migration method for receiver function imaging: 2. Application to the Japan subduction zone. *J. Geophys. Res. Solid Earth* 110 (B11). doi:10.1029/2005jb003666

Chen, Y., Li, W., Yuan, X., Badal, J., and Teng, J. (2015). Tearing of the Indian lithospheric slab beneath southern Tibet revealed by SKS-wave splitting measurements. *Earth Planet. Sci. Lett.* 413, 13–24. doi:10.1016/j.epsl.2014.12.041

Chevalier, M. L., Tapponnier, P., van der Woerd, J., Leloup, P., Wang, S., Pan, J., et al. (2020). Late quaternary extension rates across the northern half of the yadong-Gulu Rift: implication for east-west extension in southern Tibet. *J. Geophys. Res. Solid Earth* 125 (7), e2019JB019106.

Clark, M. K., and Royden, L. H. (2000). Topographic ooze: building the eastern margin of Tibet by lower crustal flow. *Geology* 28 (8), 703–706. doi:10.1130/0091-7613(2000)028<0703:tobtem>2.3.co;2

Ding, L., Zhong, D., Yin, A., Kapp, P., and Harrison, T. M. (2001). Cenozoic structural and metamorphic evolution of the eastern Himalayan syntaxis (Namche Barwa). *Earth Planet. Sci. Lett.* 192 (3), 423–438. doi:10.1016/s0012-821x(01)00463-0

England, P., and Houseman, G. (1989). Extension during continental convergence, with application to the Tibetan Plateau. *J. Geophys. Res. Solid Earth* 94 (12), 17561–17579. doi:10.1029/jb094ib12p17561

Farrell, J., Wu, S. M., Ward, K. M., and Lin, F. C. (2018). Persistent noise signal in the FairfieldNodal three-component 5-hz geophones. *Seismol. Res. Lett.* 89 (5), 1609–1617. doi:10.1785/0220180073

Gan, W., Zhang, P., Shen, Z. K., Niu, Z., Wang, M., Wan, Y., et al. (2007). Present-day crustal motion within the Tibetan Plateau inferred from GPS measurements. *J. Geophys. Res. Solid Earth* 112 (B8), B08416. doi:10.1029/2005jb004120

Guo, X., Gao, R., Zhao, J., Xu, X., Lu, Z., Klemperer, S. L., et al. (2018). Deep-seated lithospheric geometry in revealing collapse of the Tibetan Plateau. *Earth-Science Rev.* 185, 751–762. doi:10.1016/j.earscirev.2018.07.013

Guo, Z., Wilson, M., Zhang, M., Cheng, Z., and Zhang, L. (2015). Post-collisional ultrapotassic mafic magmatism in south Tibet: products of partial melting of pyroxenite in the mantle wedge induced by roll-back and delamination of the subducted Indian continental lithosphere slab. *J. Petrology* 56 (7), 1365–1406. doi:10.1093/petrology/egv040

Ha, G., Wu, Z., and Liu, F. (2019). Late quaternary vertical slip rates along the southern yadong–gulu rift, southern Tibetan plateau. *Tectonophysics* 755, 75–90. doi:10.1016/j.tecto.2019.02.014

Hager, C. (2014). Integrated tectonic and quantitative thermochronometric investigation of the Xainza rift. Tibet Dissertation. University of Kansas.

Harrison, T. M., Copeland, P., Kidd, W., and Lovera, O. M. (1995). Activation of the Nyainqentanghla shear zone: implications for uplift of the southern Tibetan plateau. *Tectonics* 14 (3), 658–676. doi:10.1029/95TC00608

Hou, Z., Zhao, Z., Gao, Y., Yang, Z., and Jiang, W. (2006). Tearing and dischronal subducting of the Indian continental slab: evidence from cenozoic gangdese volcano-magmatic rocks in south Tibet. *Acta Petrol. Sin.* 22 (4), 761–774.

Huchon, P., Pichon, X. L., and Rangin, C. (1994). Indochina peninsula and the collision of India and Eurasia. *Geology* 22 (1), 27–30. doi:10.1130/0091-7613(1994)022<0027:ipatco>2.3.co;2

Kapp, J. L. D. A. (2005). Nyainqentanglha Shan: A window into the tectonic, thermal, and geochemical evolution of the Lhasa block, southern Tibet. *J. Geophys. Res.* 110 (B8), B08413. doi:10.1029/2004jb003330

Kumar, P., Yuan, X., Kind, R., and Ni, J. (2006). Imaging the colliding Indian and Asian lithospheric plates beneath Tibet. *J. Geophys. Res. Solid Earth* 111 (B6). doi:10.1029/2005jb003930

Langston, C. A. (1979). Structure under Mount Rainier, Washington, inferred from teleseismic body waves. *J. Geophys. Res.* 84 (B9), 4749. doi:10.1029/jb084ib09p04749

Laskowski, A. K., Orme, D. A., Cai, F., and Ding, L. (2019). The ancestral Lhasa river: A late cretaceous trans-arc river that drained the proto–Tibetan plateau. *Geology* 47 (11), 1029–1033. doi:10.1130/g46823.1

Leahy, G. M., Saltzer, R. L., and Schmedes, J. (2012). Imaging the shallow crust with teleseismic receiver functions. *Geophys. J. Int.* 191 (2), 627–636. doi:10.1111/j.1365-246X.2012.05615.x

Lease, R. O., Burbank, D. W., Clark, M. K., Farley, K. A., Zheng, D., and Zhang, H. (2011). Middle Miocene reorganization of deformation along the northeastern Tibetan Plateau. *Geology* 39 (4), 359–362. doi:10.1130/g31356.1

Li, C., Van der Hilst, R. D., Meltzer, A. S., and Engdahl, E. R. (2008). Subduction of the Indian lithosphere beneath the Tibetan Plateau and Burma. *Earth Planet. Sci. Lett.* 274 (1-2), 157–168. doi:10.1016/j.epsl.2008.07.016

Liang, S., Gan, W., Shen, C., Xiao, G., Liu, J., Chen, W., et al. (2013). Three-dimensional velocity field of present-day crustal motion of the Tibetan Plateau derived from GPS measurements. *J. Geophys. Res. Solid Earth* 118 (10), 5722–5732. doi:10.1002/2013jb010503

Liang, X., Chen, Y., Tian, X., Chen, Y. J., Ni, J., Gallegos, A., et al. (2016). 3D imaging of subducting and fragmenting Indian continental lithosphere beneath southern and central Tibet using body-wave finite-frequency tomography. *Earth Planet. Sci. Lett.* 443, 162–175. doi:10.1016/j.epsl.2016.03.029

Liu, G., Persaud, P., and Clayton, R. W. (2018). Structure of the northern Los Angeles basins revealed in teleseismic receiver functions from short-term nodal seismic arrays. *Seismol. Res. Lett.* 89 (5), 1680–1689. doi:10.1785/0220180071

Liu, Z.-C., Wu, F.-Y., Ji, W.-Q., Wang, J.-G., and Liu, C.-Z. (2014). Petrogenesis of the Ramba leucogranite in the Tethyan Himalaya and constraints on the channel flow model. *Lithos* 208-209, 118–136. doi:10.1016/j.lithos.2014.08.022

Liu, Z., Tian, X., Gao, R., Wang, G., Wu, Z., Zhou, B., et al. (2017). New images of the crustal structure beneath eastern Tibet from a high-density seismic array. *Earth Planet. Sci. Lett.* 480, 33–41. doi:10.1016/j.epsl.2017.09.048

Maheo, G., Leloup, P., Valli, F., Lacassin, R., Arnaud, N., Paquette, J., et al. (2007). Post 4 Ma initiation of normal faulting in southern Tibet. Constraints from the Kung Co half graben. *Earth Planet. Sci. Lett.* 256 (1-2), 233–243. doi:10.1016/j.epsl.2007.01.029

Pan, Y., and Kidd, W. (1992). Nyainqentanglha shear zone: A late Miocene extensional detachment in the southern Tibetan plateau. *Geology* 20 (9), 775–778. doi:10.1130/0091-7613(1992)020<0775:nszalm>2.3.co;2

Pubellier, M., and Morley, C. (2014). The basins of sundaland (SE Asia): evolution and boundary conditions. *Mar. Petroleum Geol.* 58, 555–578. doi:10.1016/j.marpetgeo.2013.11.019

Replumaz, A., Guillot, S., Villaseñor, A., and Negredo, A. M. (2013). Amount of Asian lithospheric mantle subducted during the India/Asia collision. *Gondwana Res.* 24 (3-4), 936–945. doi:10.1016/j.gr.2012.07.019

Ringler, A. T., Anthony, R. E., Karplus, M. S., Holland, A. A., and Wilson, D. C. (2018). Laboratory tests of three Z-land Fairfield nodal 5-hz, three-component sensors. *Seismol. Res. Lett.* 89 (5), 1601–1608. doi:10.1785/0220170236

Royden, L. H., Burchfiel, B. C., King, R. W., Wang, E., Chen, Z., Shen, F., et al. (1997). Surface deformation and lower crustal flow in eastern Tibet. *Science* 276 (5313), 788–790. doi:10.1126/science.276.5313.788

Saikia, S., Chopra, S., Baruah, S., and Singh, U. (2017). Shallow sedimentary structure of the brahmaputra valley constraint from receiver functions analysis. *Pure Appl. Geophys.* 174, 229–247. doi:10.1007/s00024-016-1371-3

Schellart, W., Chen, Z., Strak, V., Duarte, J., and Rosas, F. (2019). Pacific subduction control on Asian continental deformation including Tibetan extension and eastward extrusion tectonics. *Nat. Commun.* 10 (1), 4480. doi:10.1038/s41467-019-12337-9

Schulze, N. (2021). *The sedimentary and tectonic evolution of the nam Co basin, Tibetan plateau, since the middle pleistocene [dissertation*. Bremen: University of Bremen.

Shapiro, N. M., Ritzwoller, M. H., Molnar, P., and Levin, V. (2004). Thinning and flow of Tibetan crust constrained by seismic anisotropy. *Science* 305 (5681), 233–236. doi:10.1126/science.1098276

Shi, D., Wu, Z., Klemperer, S. L., Zhao, W., Xue, G., and Su, H. (2015). Receiver function imaging of crustal suture, steep subduction, and mantle wedge in the eastern India–Tibet continental collision zone. *Earth Planet. Sci. Lett.* 414, 6–15. doi:10.1016/j.epsl.2014.12.055

Spicer, R. A., Harris, N. B., Widdowson, M., Herman, A. B., Guo, S., Valdes, P. J., et al. (2003). Constant elevation of southern Tibet over the past 15 million years. *Nature* 421 (6923), 622–624. doi:10.1038/nature01356

Sweet, J. R., Anderson, K. R., Bilek, S., Brudzinski, M., Chen, X., Deshon, H., et al. (2018). A community experiment to record the full seismic wavefield in Oklahoma. *Seismol. Res. Lett.* 89 (5), 1923–1930. doi:10.1785/0220180079

Tapponnier, P., Zhiqin, X., Roger, F., Meyer, B., Arnaud, N., Wittlinger, G., et al. (2001). Oblique stepwise rise and growth of the Tibet Plateau. *Science* 294 (5547), 1671–1677. doi:10.1126/science.105978

Tian, X., Chen, Y., Tseng, T.-L., Klemperer, S. L., Thybo, H., Liu, Z., et al. (2015). Weakly coupled lithospheric extension in southern Tibet. *Earth Planet. Sci. Lett.* 430, 171–177. doi:10.1016/j.epsl.2015.08.025

Tian, X., Bai, Z., Klemperer, S. L., Liang, X., Liu, Z., Wang, X., et al. (2021). Crustal-scale wedge tectonics at the narrow boundary between the Tibetan Plateau and Ordos block. *Earth Planet. Sci. Lett.* 554, 116700. doi:10.1016/j.epsl.2020.116700

Todrani, A., Speranza, F., D'Agostino, N., and Zhang, B. (2022). Post-50 Ma evolution of India-Asia collision zone from paleomagnetic and GPS data: greater India indentation to eastward Tibet flow. *Geophys. Res. Lett.* 49 (1), e2021GL096623. doi:10.1029/2021gl096623

Wang, G., Wei, W., Ye, G., Jin, S., Jing, J., Zhang, L., et al. (2017). 3-D electrical structure across the yadong-gulu rift revealed by magnetotelluric data: new insights on the extension of the upper crust and the geometry of the underthrusting Indian lithospheric slab in southern Tibet. *Earth Planet. Sci. Lett.* 474, 172–179. doi:10.1016/j.epsl.2017.06.027

Ward, K. M., and Lin, F. C. (2017). On the viability of using autonomous three-component nodal geophones to calculate TeleseismicPsReceiver functions with an application to old faithful, yellowstone. *Seismol. Res. Lett.* 88 (5), 1268–1278. doi:10.1785/0220170051

Ward, K. M., Lin, F., and Schmandt, B. (2018). High-resolution receiver function imaging across the cascadia subduction zone using a dense nodal array. *Geophys. Res. Lett.* 45 (22), 218–212. doi:10.1029/2018gl079903

Wu, S. M., Ward, K. M., Farrell, J., Lin, F. C., Karplus, M., and Smith, R. B. (2017). Anatomy of old faithful from subsurface seismic imaging of the yellowstone upper geyser basin. *Geophys. Res. Lett.* 44 (20), 10,240–10,247. doi:10.1002/2017gl075255

Xu, Z., Ji, S., Cai, Z., Zeng, L., Geng, Q., and Cao, H. (2012). Kinematics and dynamics of the Namche barwa syntaxis, eastern himalaya: constraints from deformation, fabrics and geochronology. *Gondwana Res.* 21 (1), 19–36. doi:10.1016/j.gr.2011.06.010

Zhang, L., Liang, S., Yang, X., Gan, W., and Dai, C. (2021). Geometric and kinematic evolution of the Jiali fault, eastern Himalayan Syntaxis. *J. Asian Earth Sci.* 212, 104722. doi:10.1016/j.jseaes.2021.104722

Zhang, Z., Chen, Y., Yuan, X., Tian, X., Klemperer, S. L., Xu, T., et al. (2013). Normal faulting from simple shear rifting in South Tibet, using evidence from passive seismic profiling across the Yadong-Gulu Rift. *Tectonophysics* 606, 178–186. doi:10.1016/j.tecto.2013.03.019

Zhao, J., Yuan, X., Liu, H., Kumar, P., Pei, S., Kind, R., et al. (2010). The boundary between the Indian and Asian tectonic plates below Tibet. *Proc. Natl. Acad. Sci.* 107 (25), 11229–11233. doi:10.1073/pnas.1001921107

Zhu, D.-C., Zhao, Z.-D., Niu, Y., Mo, X.-X., Chung, S.-L., Hou, Z.-Q., et al. (2011). The Lhasa terrane: record of a microcontinent and its histories of drift and growth. *Earth Planet. Sci. Lett.* 301 (1-2), 241–255. doi:10.1016/j.epsl.2010.11.005

Zhu, L. (2000a). Crustal structure across the San Andreas Fault, southern California from teleseismic converted waves. *Earth Planet. Sci. Lett.* 179 (1), 183–190. doi:10.1016/S0012-821x(00)00101-1

Zuo, J., Wu, Z., Ha, G., Hu, M., Zhou, C., and Gai, H. (2021). Spatial variation of nearly NS-trending normal faulting in the southern yadong-gulu rift, Tibet: new constraints from the chongba yumtso fault, duoqing Co graben. *J. Struct. Geol.* 144, 104256. doi:10.1016/j.jsg.2020.104256